Secreted dengue virus NS1 is predominantly dimeric and in complex with high-density lipoprotein

Bing Liang Alvin Chew[1,2]†, An Qi Ngoh [3]†, Wint Wint Phoo[4]†, Kitti Wing Ki Chan[3], Zheng Ser[4], Shiao See Lim [3], Meng Jie Grace Weng[1,2], Satoru Watanabe[3], Milly M. Choy[3], Jenny G. Low[3,6], Eng Eong Ooi[3,7,8], Radoslaw M. Sobota[4], Subhash G. Vasudevan[3,5,9]*, Dahai Luo[1,2]*

Affiliations:

[1]Lee Kong Chian School of Medicine, Nanyang Technological University; EMB 03-07, 59 Nanyang Drive, Singapore 636921

[2]NTU Institute of Structural Biology, Nanyang Technological University; EMB 06-01, 59 Nanyang Drive, Singapore 636921, Singapore

[3]Program in Emerging Infectious Diseases, Duke-NUS Medical School; 8 College Road, Singapore 169857, Singapore

[4]Functional Proteomics Laboratory, Institute of Molecular and Cell Biology, Agency for Science, Technology and Research (A*STAR); 61 Biopolis Drive, Proteos, Singapore 138673, Singapore

[5]Department of Microbiology and Immunology, National University of Singapore; 5 Science Drive 2, Singapore 117545, Singapore

[6]Department of Infectious Diseases, Singapore General Hospital, Singapore, Singapore.

[7]Yong Loo Lin School of Medicine, National University of Singapore, Singapore, Singapore.

[8]Saw Swee Hock School of Public Health, National University of Singapore, Singapore, Singapore.

[9]Institute for Glycomics (G26), Griffith University Gold Coast Campus, QLD 4222, Australia.

† These three authors contributed equally to the work.

*Corresponding author. Email: subhash.vasudevan@duke-nus.edu.sg (S.V.); luodahai@ntu.edu.sg (D.L.)

Abstract

Severe dengue infections are characterized by endothelial dysfunction shown to be associated with the secreted nonstructural protein 1 (sNS1), making it an attractive vaccine antigen and biotherapeutic target. To uncover the biologically relevant structure of sNS1, we extracted the native form of sNS1 from cells infected with either the DENV WT or T164S mutant whose appearance was associated with a dengue outbreak in Cuba. We determined the cryoEM structures of sNS1 and its complex with a monoclonal antibody/Fab and found that the major species of sNS1 is a 1:1 complex of the NS1 dimer embedded in a High Density Lipoprotein (HDL) particle. Cross-linking MS studies confirm NS1:ApoA1 dimer formation with most ApoA1 interaction sites mapped to the NS1 wing and hydrophobic domains. Our results shed fresh light on the molecular pathogenesis of dengue and may have broad implications for managing dengue infection.

Summary

CryoEM structures of secreted dengue virus NS1 protein reveal dimers in complex with high-density lipoprotein.

Main Text

Dengue virus (DENV) is a member of the flaviviruses genus that is causing significant healthcare problems and economic burden worldwide, partially due to the lack of effective therapeutics and the limited efficacy of the only licensed vaccine, Dengvaxia. The viral nonstructural protein 1 (NS1) is a highly conserved and multifunctional protein that exists in both intracellular and secreted forms during viral infection (*1*). Inside the infected cells, NS1 is found in the ER lumen as an essential part of the membranous viral RNA replication compartment. Upon release from the cells, NS1 enters the blood circulation where laboratory experiments suggest that it could induce plasma leakage, a hallmark of severe dengue, either independently (*2*) or through inducing pro-inflammatory responses (*3*).

Mature NS1 is 352 amino acids long with an apparent molecular mass between 40 – 50 kDa depending on its glycosylation state at asparagine residues 130 and 207 for the majority of flaviviruses (*4*). All flavivirus NS1 species contain 12 conserved cysteine residues that form six intra-chain disulphide bonds, two at the N-terminus and four at the C-terminus, that are crucial for non-covalent dimer formation which remain stable to reduction but are heat-labile (*5*). NS1 has a three-domain architecture, a hydrophobic β-roll (residues 1-29), an a/b wing (38-151), and a β-ladder (181-352). The connector segments between the wing and β-ladder domains, residues 30-37 and 152-180, form a 3-stranded β-sheet. The dimer has a distinct crossed shape with the wings extending from the central β-ladder which has an extended β-sheet that faces the β-roll and a ‘‘spaghetti loop” on the opposite hydrophilic outer face that lacks structured elements (*6-8*). The secreted NS1 (sNS1) is reported to be a barrel-shaped hexamer with lipid cargo held together by hydrophobic interactions based on biophysical and low-resolution EM analysis (*9-11*). The N-linked glycans at asparagine residues 130 and 207 were also shown to be critical for stabilizing the secreted hexamer for secretion and extracellular protein stability (*12*). The hexameric structure modelled based on the crystal lattice contacts also appears to be consistent with the 30 □ cryo-EM map (*6, 13*). While earlier studies used cross-linkers to demonstrate the hexamer conformation, it remains unclear how the hexameric form is biologically meaningful from its assembly to the disruption of endothelial glycocalyx at the membrane milieu. The hexamer model is based on several untested assumptions and low resolution EM data that were challenged by recent evidence that suggests that NS1 may be associated with HDL (*14, 15*) and uses scavenger receptor B1 as a cell receptor in cultured cells (*16*). To reconcile the findings

related to the functional forms of sNS1 and better understand its biological roles, we obtain the native form of sNS1 from the cell-based virus infection system and determine its structures with an antibody.

Results

To obtain a close mimic of sNS1 circulating in dengue fever patients' sera, we immunoaffinity purified sNS1 from the FBS-supplemented culture supernatant of DENV2 WT (sNS1wt) or T164S mutant (sNS1ts) virus-infected Vero cells (Fig. 1 and S1). The T164S mutation in the greasy finger loop of the wing and β-ladder interdomain of NS1 was identified from a severe DENV2 epidemic in Cuba in 1997, where a correlation with enhanced clinical disease severity was observed (*17*). We recently demonstrated that this single mutation in NS1 could directly cause lethality in mice and also increase sNS1 secretion (*18*), the latter being an attractive consideration for its inclusion in this study to provide higher quantities of sNS1 for structural studies.

Both purified sNS1wt and sNS1ts retained a molecular size of approximately 250 kDa as detected with anti-NS1 56.2 monoclonal antibody (Ab56.2; (*19, 20*)) following separation on a Native-PAGE (Fig. 1A), as previously reported (*18*). On a reducing SDS-PAGE, we identified two major bands of approximately 50 kDa and 25 kDa for both sNS1wt and sNS1ts (Fig. 1B). While the 50 kDa band corresponds to the recombinant NS1 (rNS1) purified from a baculovirus expression system in SF9 cells (*19*), the identity of the 25 kDa band was unknown (Fig. 1B). Preliminary mass ID suggested that this could be apolipoprotein A1 (ApoA1), a major component of HDL, which has a calculated molecular weight of 28 kDa (*21*). In this study, we first confirmed the identity of the two bands as NS1 and ApoA1 respectively by western blot (Fig. 1C). Next, to determine the composition of the prominent 250 kDa band in the Native-PAGE that has been associated with hexameric sNS1 in several structural studies (*9-11*), we excised the 250 kDa and 100 kDa protein bands from sNS1wt and sNS1ts, the latter being present only in sNS1ts, for protein identification by LC-MS (Fig. 1 D-E). The total elute fraction and its 50 kDa and 25 kDa bands from a reducing SDS-PAGE (Fig. 1B) were also excised as positive controls. Surprisingly, 250 kDa bands from both sNS1wt (Fig. 1D) and sNS1ts (Fig. 1E) showed the presence of both NS1 and ApoA1. The 100 kDa band from sNS1ts and the 25kDa

band from reducing SDS-PAGE contained only ApoA1. Previous protein gel analysis showed that HDL is predominantly homodimeric ApoA1 (*22*) and this was further confirmed by zero-length chemical cross-linking mass spectrometry (XL-MS) to be ApoA1 antiparallel dimers centered on both helix 5 in the monomers along a left-left (LL5/5) interface with two-fold axis symmetry (*23*). Together, these results indicate that the ~250 kDa sNS1 as shown in Figure 1A is a complex of the NS1 protein and ApoA1/HDL.

Next, to gain molecular insights into the sNS1 complex, we used cryoEM to determine the native structure of sNS1. The data collection statistics and data processing workflow are summarized in Table S1 and Figure S2 respectively. sNS1ts alone was initially observed to have no discernible features beyond a spherical-like density with varying dimensions averaging around 106 Å by 77 Å (Fig. S2, in grey, and Fig. S3A). To obtain high-resolution structural information on the complex, we proceeded to collect data for the ternary complexes of the sNS1wt:Ab56.2 and the sNS1wt:Fab56.2 (Fig. 2A and Fig S2, depicted in red and blue respectively), a well-proven approach for solving the structures of small proteins (*24, 25*). Overall, both samples resulted in similarly distinguishable 2D class averages (Fig 2B-C) which show the Fab binding to the cross-shaped NS1 that is associated with a lower-density sphere. In the sNS1wt: Fab56.2 ternary complex dataset, we further observed two apparent but rare sub-classes of free sNS1wt bound to two units of Fab56.2 representing only 3.5% of the total population of picked particles (Fig. 2C, red dashed boxes) and it has a disproportionately higher number of free sNS1wt particles (2D averages are not shown) compared to the sNS1wt:Ab56.2. Both cryoEM map reconstructions could be fitted with the NS1 dimer and Fab56.2 structures (Fig. 2D) predicted separately using AlphaFold (*26*) with a correlation value of 0.75 to the fitted regions using a simulated map from atoms of NS1 dimer and Fab at 5 Å. The Fab is observed to bind to the β-ladder domain and the approximate dimensions of the spherical-like HDL could also be measured with more confidence at 82 Å by 65 Å (Fig. S2, in red).

Similarly, we also determined the structures of the ternary complex of sNS1ts mutant with Fab56.2 (Fig. 3A). Interestingly, 2D class averages of sNS1ts:Fab56.2 dataset showed a significant sub-population of free NS1ts bound with two units of Fab56.2 (53.7%), in addition to the HDL spheres (23.6%) and Fab:sNS1ts (22.7%) classes (Fig. 3B). This allowed the

reconstruction of the free NS1ts:Fab complex cryoEM map besides the sNS1ts form (Fig. S2, depicted in green). The NS1ts dimer and Fab56.2 predicted structures could be fitted in with an overall correlation value of 0.3 using map simulated from atoms at 5 Å (Fig. 3C). Achieving atomic resolution remains a challenge due to preferred orientation (Fig. S3D) and alignment issue which is evident in the steric clashes at the Fab binding interface with the NS1 β-ladder domain (Fig. 3C, inset). Between the density maps of free NS1ts: Fab (Fig. 3D, grey) and sNS1ts:Fab ternary complex (Fig. 3D, yellow) fitted with a correlation value of 0.7137 based on NS1 map region, the inset highlights the rotation of the Fab from the free NS1 dimer to the HDL-bound sNS1. Further comparison of sNS1ts: Fab ternary complex with the density map of sNS1wt: Fab ternary complex (Fig. 3D, purple) shows an agreement of the HDL-bound conformation that is distinct from the free NS1:Fab form. Overall, the cryoEM results provided direct unequivocal evidence that the ~250 kDa sNS1 from infected cells is a complex of NS1 dimer and HDL. The dimeric NS1 appears semi-embedded on an HDL particle through its hydrophobic surface, with a conformation that only exposes one end of the β-ladder domain to which the tested antibody could bind. This asymmetrical binding raises two possibilities: (1) The sNS1 complex is simply based on hydrophobic protein-lipid interactions; or (2) there are additional direct interactions between NS1 and ApoA1 protein.

To further refine our understanding of the sNS1 complex, we probed the interaction between NS1 and ApoA1 (Fig. S4A-B) with XL-MS. We identified a total of 28 NS1-NS1 crosslinks, 29 ApoA1-ApoA1 crosslinks, and 25 NS1-ApoA1 inter-molecular crosslinks (Fig. 4A). The identified crosslinks were further mapped to the structural model of sNS1 and the predicted ApoA1 structure. The first 58 residues of ApoA1 were removed from the 3D model prediction for clarity as the N-terminal domain of ApoA1 is flexible (*22*). Notably, 23 out of 28 intra-NS1 crosslinks are located on the β-roll and wing domains (Fig. 4B-C), and the NS1-ApoA1 inter-molecular crosslinks are located between the β-roll and wing domains of NS1 and the helices 3, 4, 8 and 10 of ApoA1 (Fig. 4A-B, D). The NS1 dimer and ApoA1 structures were fitted into the cryoEM density map of sNS1wt:Fab ternary complex (Fig. 4E) and the intra- and inter-molecular distances between Cα backbone atoms were measured to determine if the distances measured are within the 30 Å cut-off for DSSO crosslinker length (*27*). Indeed, a total of 24 out of 28 intramolecular crosslinks within dimeric sNS1 and 18 out of 29 intramolecular crosslinks within

ApoA1 as well as 18 out of 25 intermolecular crosslinks between dimeric sNS1 and ApoA1 have less than 30 Å distance between Cα. Taken together, the intermolecular interaction residues identified using in-solution XL-MS (Fig. 4B) do support the fitted 3D model of sNS1wt: Fab ternary complex (Fig. 4E). Although there were fewer crosslink sites in sNS1ts than sNS1wt (Fig. S4C-E), the models derived from XL-MS and cryoEM of sNS1ts were similar to that of sNS1wt. It is possible that the dimeric NS1 (~100 kDa) assembles as a complex with HDL composed of ApoA1 homodimers (~100 kDa) arranged as antiparallel to result in the ~250 kDa band that was thought to be hexameric NS1 **(*9-11*)**. We further examined the feasibility of the hexamer model by building a sphere with a radius of 30 Å which represents the maximum range between the Cα atoms that can be crosslinked, centered at the Cα of Ser2 residue on the β-roll (Fig. S5A). In the hexamer model, this sphere is fully entrapped within the central cavity, which renders the intermolecular interactions between NS1 and ApoA1 incompatible and therefore unlikely.

Discussion

The high-resolution crystal structures of NS1 dimer from full-length DENV and WNV (*6*) derived from recombinant insect-cell expression provided a definitive architecture of NS1. They revealed its unique structure and features that could interact with a myriad of proteins associated with its immune evasion and virotoxin roles (*28*), interactions with viral E protein (*29*) and the NS4A-2K-NS4B precursor protein (*30*) that are important in virus production and replication respectively. Prior to that, sNS1 from DENV1-infected cells was shown to be a detergent-labile complex of ~300 kDa suggested to be a hexameric NS1 oligomer based on results obtained from SEC, SAXS, chemical crosslinking, and negative staining EM methods (*9*). 3D reconstruction of sNS1 at ~30 Å resolution using the cryoEM method provided a low-resolution model of the hexameric NS1 as an open barrel shape with a prominent central channel along the axis of the three-fold symmetry filled with lipids that showed a similar lipid-cargo profile as HDL (*10*). Coincidentally, the NS1 hexamer model based on the crystal packing symmetry and the negative staining EM images of the detergent-free NS1 protein seemed to suggest that the hexameric NS1 of the same conformation can be recapitulated *in vitro* (*6*). While these previous studies have pointed to a feasible model of the hexameric sNS1 that is organized as a trimer of NS1 dimers

and filled with lipid cargo at the hydrophobic central cavity, how sNS1 hexamer forms and how sNS1 may cause vascular leakage remains elusive.

By using combinatory approaches of LC-MS, cryoEM and XL-MS, we have defined the molecular composition and architecture of the purified infection-derived sNS1 complex. sNS1 has been shown to exist as dimers on the cell surface membrane (*31*). Hence, it is plausible that dimeric NS1 could be picked up and chaperoned by HDL particles, which are conventionally involved in reverse cholesterol transport from peripheral tissues to the liver (*32*), as stable complexes for circulation to target organs via the bloodstream. Within this complex, we found that a single copy of NS1 dimer is closely associated with the ApoA1 protein, along with a dynamic lipid load consisting of predominantly phospholipids, cholesterols and triglycerides present as part of the HDL particles (*32*). We also captured a population of free sNS1ts mutant dimers that is bound to two copies of Fab56.2. This suggests that there could be a dynamic equilibrium between the HDL-bound NS1 and free NS1, regulated by the interplay between NS1 secretion and circulating HDL. Additionally, our cryoEM structures are in agreement with a recent report of a reconstituted DENV NS1:HDL complex that showed NS1 dimers anchored at the surface of HDL particles (*15*). . Finally, the detection and quantification of NS1 from a ApoA1 pull-down using commercial antibodies in DENV1-infected patient serum (*33*) provides indirect evidence that HDL-bound NS1 complexes are also clinically relevant (Fig. S6). Our work has shed new light on the structural and molecular basis of NS1 and will be useful in guiding the future development of NS1-targeted vaccination and therapeutics strategies.

References and Notes

1. D. R. Glasner, H. Puerta-Guardo, P. R. Beatty, E. Harris, The Good, the Bad, and the Shocking: The Multiple Roles of Dengue Virus Nonstructural Protein 1 in Protection and Pathogenesis. *Annu Rev Virol* **5**, 227-253 (2018).
2. H. Puerta-Guardo, D. R. Glasner, E. Harris, Dengue Virus NS1 Disrupts the Endothelial Glycocalyx, Leading to Hyperpermeability. *PLoS Pathog* **12**, e1005738 (2016).
3. P. R. Beatty *et al.*, Dengue virus NS1 triggers endothelial permeability and vascular leak that is prevented by NS1 vaccination. *Sci Transl Med* **7**, 304ra141 (2015).
4. K. L. Carpio, A. D. T. Barrett, Flavivirus NS1 and Its Potential in Vaccine Development. *Vaccines (Basel)* **9**, (2021).
5. T. P. Wallis, C.-Y. Huang, S. B. Nimkar, P. R. Young, J. J. Gorman, Determination of the Disulfide Bond Arrangement of Dengue Virus NS1 Protein*. *Journal of Biological Chemistry* **279**, 20729-20741 (2004).

6. D. L. Akey *et al.*, Flavivirus NS1 Structures Reveal Surfaces for Associations with Membranes and the Immune System. *Science* **343**, 881-885 (2014).
7. X. Xu *et al.*, Contribution of intertwined loop to membrane association revealed by Zika virus full-length NS1 structure. *EMBO J* **35**, 2170-2178 (2016).
8. W. C. Brown *et al.*, Extended surface for membrane association in Zika virus NS1 structure. *Nature Structural & Molecular Biology* **23**, 865-867 (2016).
9. M. Flamand *et al.*, Dengue Virus Type 1 Nonstructural Glycoprotein NS1 Is Secreted from Mammalian Cells as a Soluble Hexamer in a Glycosylation-Dependent Fashion. *Journal of Virology* **73**, 6104-6110 (1999).
10. I. Gutsche *et al.*, Secreted dengue virus nonstructural protein NS1 is an atypical barrel-shaped high-density lipoprotein. *Proc Natl Acad Sci U S A* **108**, 8003-8008 (2011).
11. D. A. Muller *et al.*, Structure of the dengue virus glycoprotein non-structural protein 1 by electron microscopy and single-particle analysis. *J Gen Virol* **93**, 771-779 (2012).
12. P. Somnuke, R. E. Hauhart, J. P. Atkinson, M. S. Diamond, P. Avirutnan, N-linked glycosylation of dengue virus NS1 protein modulates secretion, cell-surface expression, hexamer stability, and interactions with human complement. *Virology* **413**, 253-264 (2011).
13. D. L. Akey, W. C. Brown, J. Jose, R. J. Kuhn, J. L. Smith, Structure-guided insights on the role of NS1 in flavivirus infection. *Bioessays* **37**, 489-494 (2015).
14. D. R. Coelho *et al.*, ApoA1 Neutralizes Proinflammatory Effects of Dengue Virus NS1 Protein and Modulates Viral Immune Evasion. *Journal of Virology* **95**, e01974-01920 (2021).
15. S. Benfrid *et al.*, The dengue virus NS1 protein conveys pro-inflammatory signals by docking onto human high-density lipoproteins. *bioRxiv*, (2021).
16. A. C. Alcala *et al.*, Dengue Virus NS1 Uses Scavenger Receptor B1 as a Cell Receptor in Cultured Cells. *J Virol* **96**, e0166421 (2022).
17. R. Rodriguez-Roche *et al.*, Virus evolution during a severe dengue epidemic in Cuba, 1997. *Virology* **334**, 154-159 (2005).
18. K. W. K. Chan *et al.*, A T164S mutation in the dengue virus NS1 protein is associated with greater disease severity in mice. *Sci Transl Med* **11**, (2019).
19. K. Rozen-Gagnon, N. J. Moreland, C. Ruedl, S. G. Vasudevan, Expression and immunoaffinity purification of recombinant dengue virus 2 NS1 protein as a cleavable SUMOstar fusion. *Protein Expr Purif* **82**, 20-25 (2012).
20. S. Watanabe *et al.*, The magnitude of dengue virus NS1 protein secretion is strain dependent and does not correlate with severe pathologies in the mouse infection model. *Journal of virology* **86**, 5508-5514 (2012).
21. C. W. K. Kitti, PhD, National University of Singapore, ScholarBank@NUS Repository (2019).
22. R. A. Silva *et al.*, Structure of apolipoprotein A-I in spherical high density lipoproteins of different sizes. *Proc Natl Acad Sci U S A* **105**, 12176-12181 (2008).
23. Y. He *et al.*, Apolipoprotein A1 Forms 5/5 and 5/4 Antiparallel Dimers in Human High-density Lipoprotein. *Molecular & Cellular Proteomics* **18**, 854-864 (2019).
24. S. Wu *et al.*, Fabs enable single particle cryoEM studies of small proteins. *Structure (London, England : 1993)* **20**, 582-592 (2012).
25. J. S. Bloch *et al.*, Structure and mechanism of the ER-based glucosyltransferase ALG6. *Nature* **579**, 443-447 (2020).

26. K. Tunyasuvunakool *et al.*, Highly accurate protein structure prediction for the human proteome. *Nature* **596**, 590-596 (2021).
27. A. Kao *et al.*, Development of a Novel Cross-linking Strategy for Fast and Accurate Identification of Cross-linked Peptides of Protein Complexes. *Molecular & Cellular Proteomics* **10**, (2011).
28. D. Watterson, N. Modhiran, P. R. Young, The many faces of the flavivirus NS1 protein offer a multitude of options for inhibitor design. *Antiviral Res* **130**, 7-18 (2016).
29. P. Scaturro, M. Cortese, L. Chatel-Chaix, W. Fischl, R. Bartenschlager, Dengue Virus Non-structural Protein 1 Modulates Infectious Particle Production via Interaction with the Structural Proteins. *PLOS Pathogens* **11**, e1005277 (2015).
30. A. Plaszczyca *et al.*, A novel interaction between dengue virus nonstructural protein 1 and the NS4A-2K-4B precursor is required for viral RNA replication but not for formation of the membranous replication organelle. *PLoS Pathog* **15**, e1007736 (2019).
31. P. Avirutnan *et al.*, Secreted NS1 of dengue virus attaches to the surface of cells via interactions with heparan sulfate and chondroitin sulfate E. *PLoS Pathog* **3**, e183 (2007).
32. A. Kontush, M. Lhomme, M. J. Chapman, Unraveling the complexities of the HDL lipidome. *Journal of Lipid Research* **54**, 2950-2963 (2013).
33. J. G. Low *et al.*, Efficacy and safety of celgosivir in patients with dengue fever (CELADEN): a phase 1b, randomised, double-blind, placebo-controlled, proof-of-concept trial. *The Lancet Infectious Diseases* **14**, 706-715 (2014).

Acknowledgments

We thank the scientific facility support from NTU Institute of Structural Biology and Protein Product Platform. We thank members of the DL and SV labs for their support.

Funding: This research is supported by the Singapore Ministry of Education under its Singapore Ministry of Education Academic Research Fund Tier 2 (T2EP30220-0020) to DL and National Medcal Research Council of Singapore (MOH-OFIRG18may-0006; MOH-OFIRG20nov-0002) to SV, A*STAR core funding and Singapore National Research Foundation under its NRF-SIS "SingMass" scheme to R.M.S, Career Development Award 2021 (A*STAR BMRC) to W.W.P., Career Development Fund 2021 (A*STAR BMRC) to S.Z., and LKCMedicine Dean's Postdoctoral Fellowship to C.B.L.A.

Author contributions: Conceptualization: SV and DL; Investigation: BLAC, AQN, WWP, KWKC, ZS, SSL, MJGW, MMC, JGL, EEO, SV and DL; Writing: BLAC, AQN, SV, and DL with input from all authors.

Competing interests: Authors declare that they have no competing interests.

Data and materials availability: EMD-#####

Figures

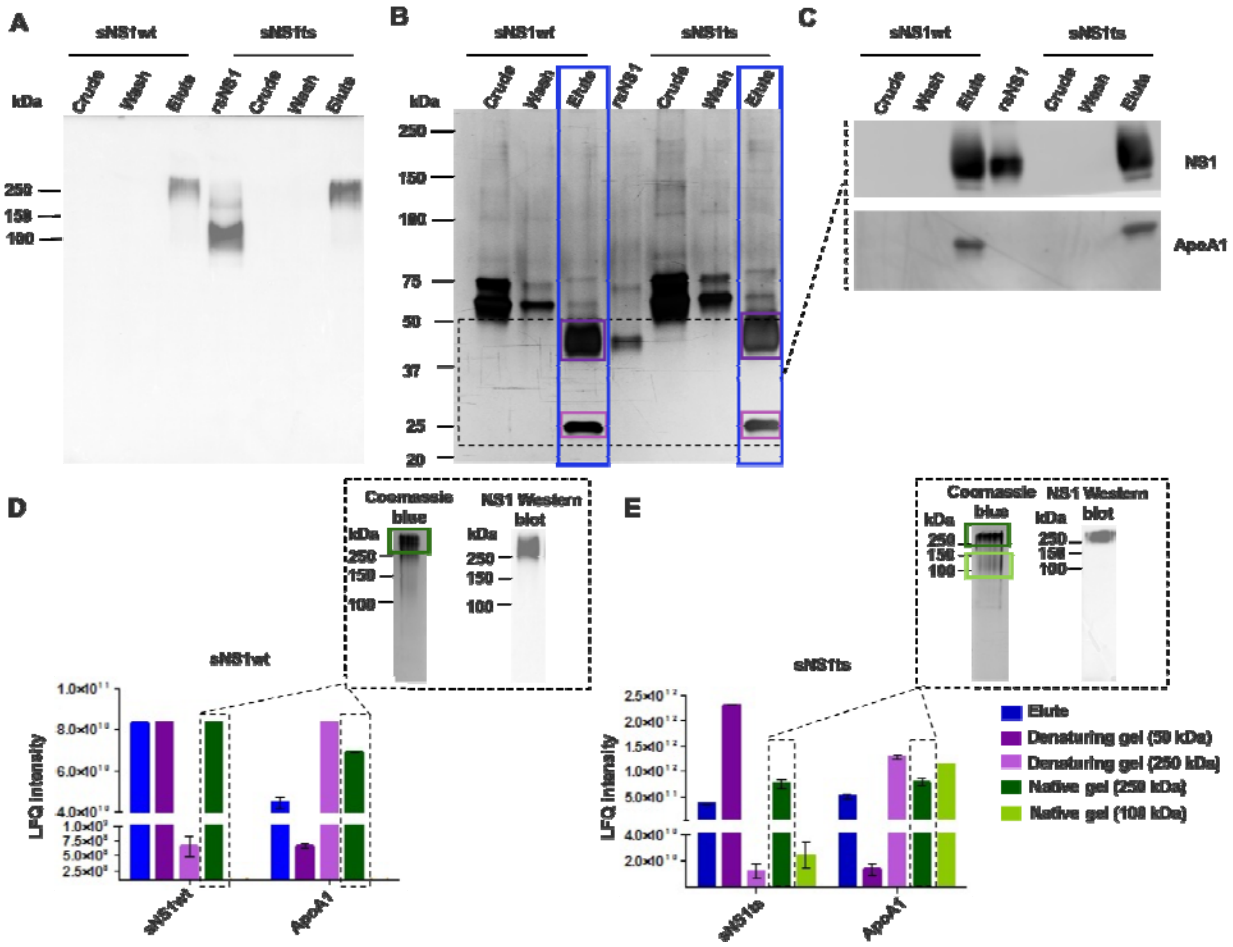

Fig. 1. Composition of the secreted NS1 from DENV-infected Vero cells. DENV 2 WT or T164S (*18*) cell culture supernatant was filtered, supplemented with protease inhibitor cocktail and 0.05% sodium azide, concentrated using a 100 kDa MWCO Vivaflow cassette and purified using 56.2 anti-NS1 antibody immunoaffinity chromatography as described previously (*19*). The eluted sNS1wt or sNS1ts was dialysed against PBS, concentrated, and stored at –80°C until further use. **(A)** Western Blot detection of sNS1wt or sNS1ts from 500 ng of total protein of Crude, Wash and Eluted immunoaffinity fractions separated on a 10% Native-PAGE. **(B)** Silver-stained gel of Crude, Wash and Eluted immunoaffinity fractions separated on a 10% SDS-PAGE gel (reducing/denaturing conditions), with recombinant baculovirus-expressed sNS1 (rsNS1) as positive control (*18-20*). **(C)** Western blot of (B) as indicated with 56.2 anti-NS1 antibody or ApoA1 antibody (Biorbyt, orb10643). **(D)** sNS1wt and **(E)** sNS1ts In-gel protein identification by liquid chromatography mass spectrometry (LC-MS). In D & E, the blue bar indicates the proteins in the eluate fraction as visualized and outlined in blue in (B). The purple and pink bars indicate the 50 kDa and 25 kDa bands outlined in the respective colours in (B) corresponding to sNS1wt/sNS1ts or ApoA1 respectively. The dark green and light green bars indicate 250 kDa and 100 kDa* (present only in sNS1ts) excised from similarly outlined bands on Native-PA gels (see inset).

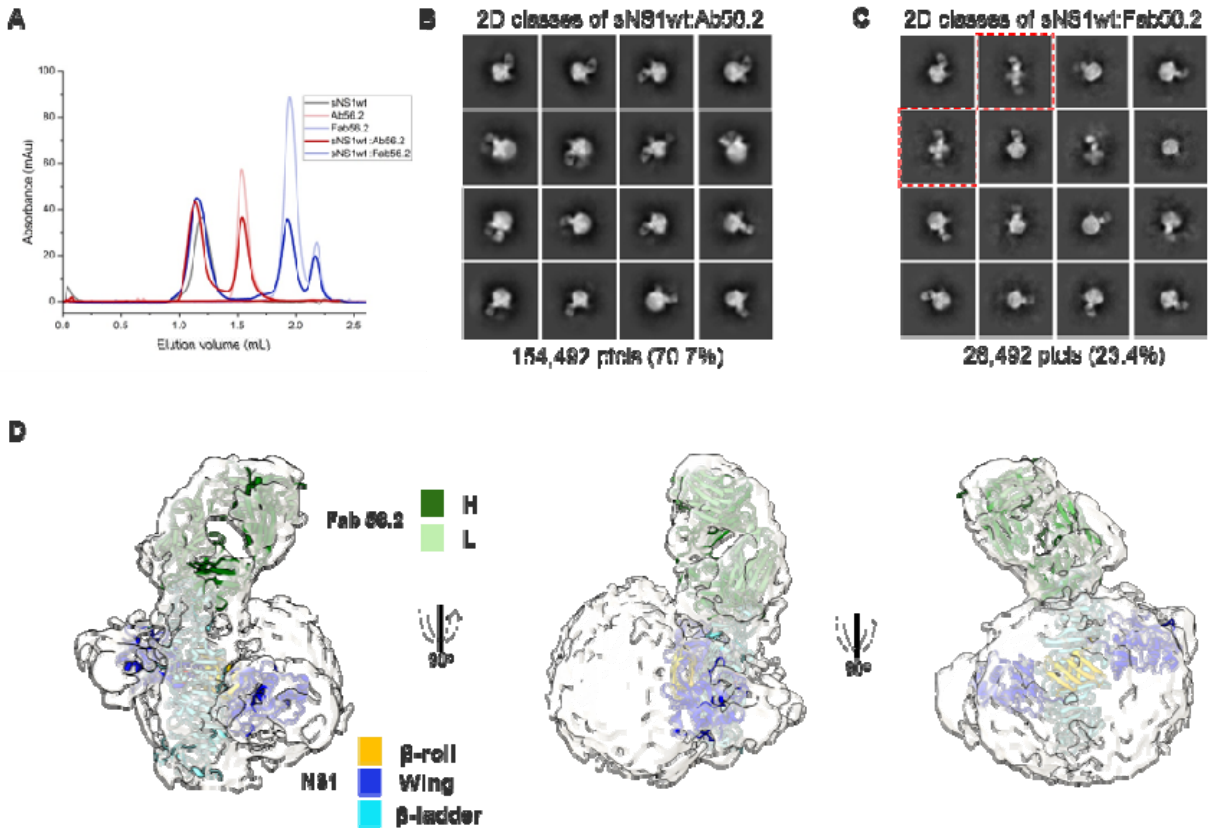

Fig. 2. CryoEM analysis of secreted NS1 in complex with non-neutralizing antibody. (A) Size exclusion chromatography was run on a Superdex 200 increase 3.2/300 GL column connected to the AKTA purifier with a flow rate of 0.075 mL/min in PBS (pH 7.4) for purified sNS1wt (gray), Ab56.2 (faded red), Fab56.2 (faded blue), sNS1wt:Ab56.2 complex and sNS1wt:Fab56.2 complex (blue). A slight leftward shift in elution volume was observed for sNS1wt upon complexing with Ab56.2 and Fab56.2. (B) sNS1wt:Ab56.2 (C) sNS1wt:Fab56.2 2D class averages showing representative sub-class of the Fab-sNS1-HDL particles. The corresponding number of particles and percentages are listed below the respective boxes. Red dashed line boxes highlight two rare views consisting of 1033 particles (3.5%) only seen in sNS1wt:Fab56.2 sample. (D) Model of sNS1wt:Fab56.2 predicted structures rigid body fitted in the Fab-sNS1-HDL CryoEM map (grey, contoured at 0.14) with correlation value of 0.75 to the fitted regions (map simulated from atoms at 5 Å). sNS1wt is coloured by its three domains, namely the β-roll (orange), wing (blue), and β-ladder (cyan). Fab56.2 is coloured by its heavy chain (dark green) and light chain (light green).

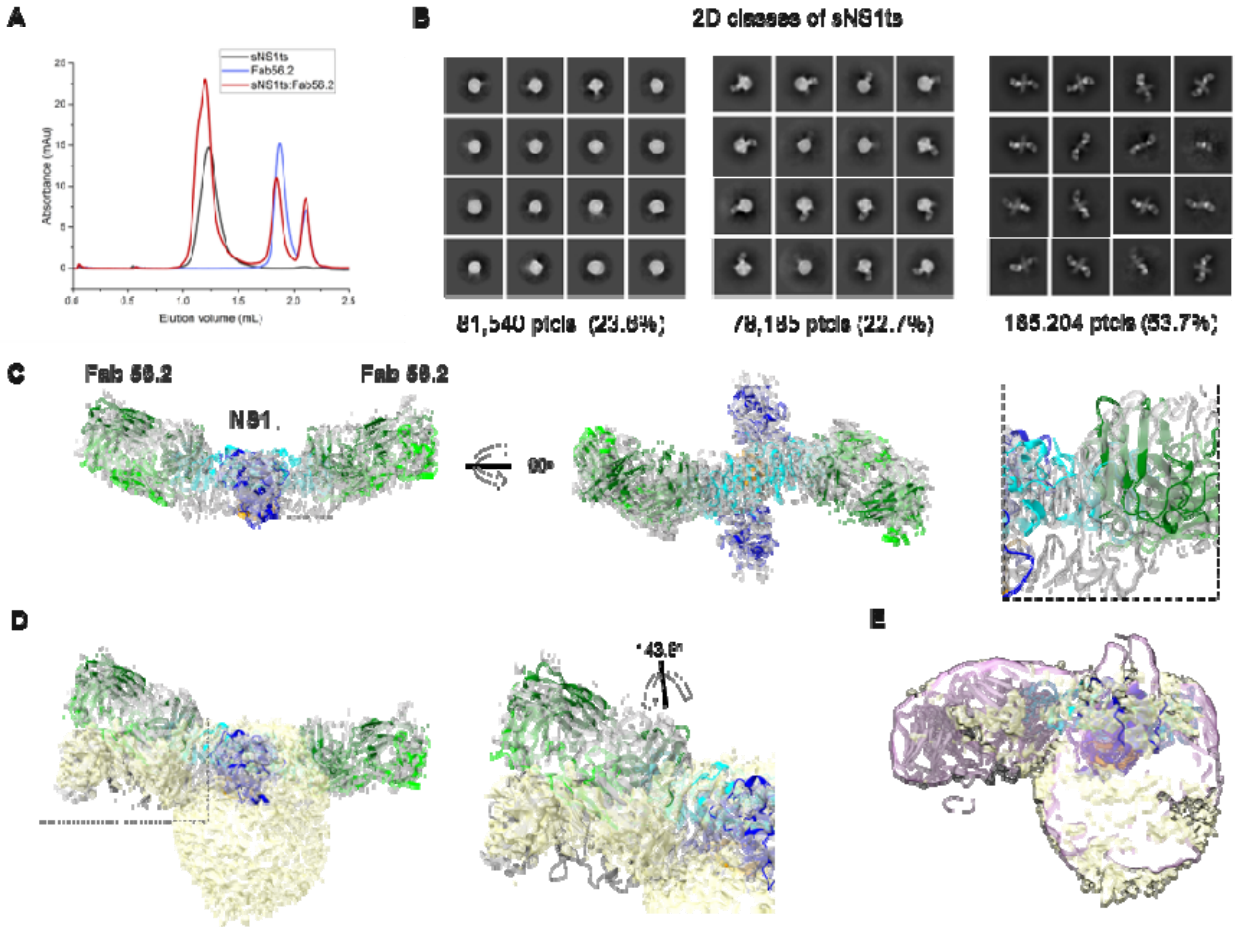

Fig. 3. Secreted NS1 forms free dimers in complex with non-neutralizing antibody. (A) Size exclusion chromatography was run on a Superdex 200 increase 3.2/300 GL column connected to the AKTA purifier with a flow rate of 0.075mL/min in PBS (pH 7.4) for purified sNS1ts (gray), Fab56.2 (faded blue) and sNS1ts:Fab56.2 (blue). A similar leftward shift in elution volume was also observed for sNS1ts upon complexing with Fab56.2. (B) 2D class averages of sNS1ts:Fab56.2 dataset which is separated into 3 distinct populations, HDL spheres, Fab-sNS1-HDL, and free Fab-sNS1. The corresponding number of particles and percentages are listed below the respective boxes. (C) Model of sNS1ts dimer and Fab56.2 predicted structures rigid body fitted in the sNS1ts:Fab56.2 density map (grey, contoured at 0.14) with correlation value of 0.3 (overall, map simulated from atoms at 5 □). sNS1ts is coloured by its three domains, namely the β-roll (orange), wing (blue), and β-ladder (cyan). Fab56.2 is coloured by its heavy chain (dark green) and light chain (light green). The inset shows a close-up view of the Fab-NS1 interface. (D) Density map fitting between NS1ts:Fab56.2 (grey, contoured at 0.14) to Fab56.2:NS1ts:HDL (yellow, contoured at 0.1) with correlation value of 0.53 (overall) and 0.7137 (on D2NS1 map region only). Inset shows the rotation of Fab from the free NS1 form to the HDL-bound form. (E) Density map fitting between Fab56.2:NS1wt:HDL (purple, contoured at 0.05) to Fab-NS1ts-HDL (yellow) with correlation value of 0.72 (overall).

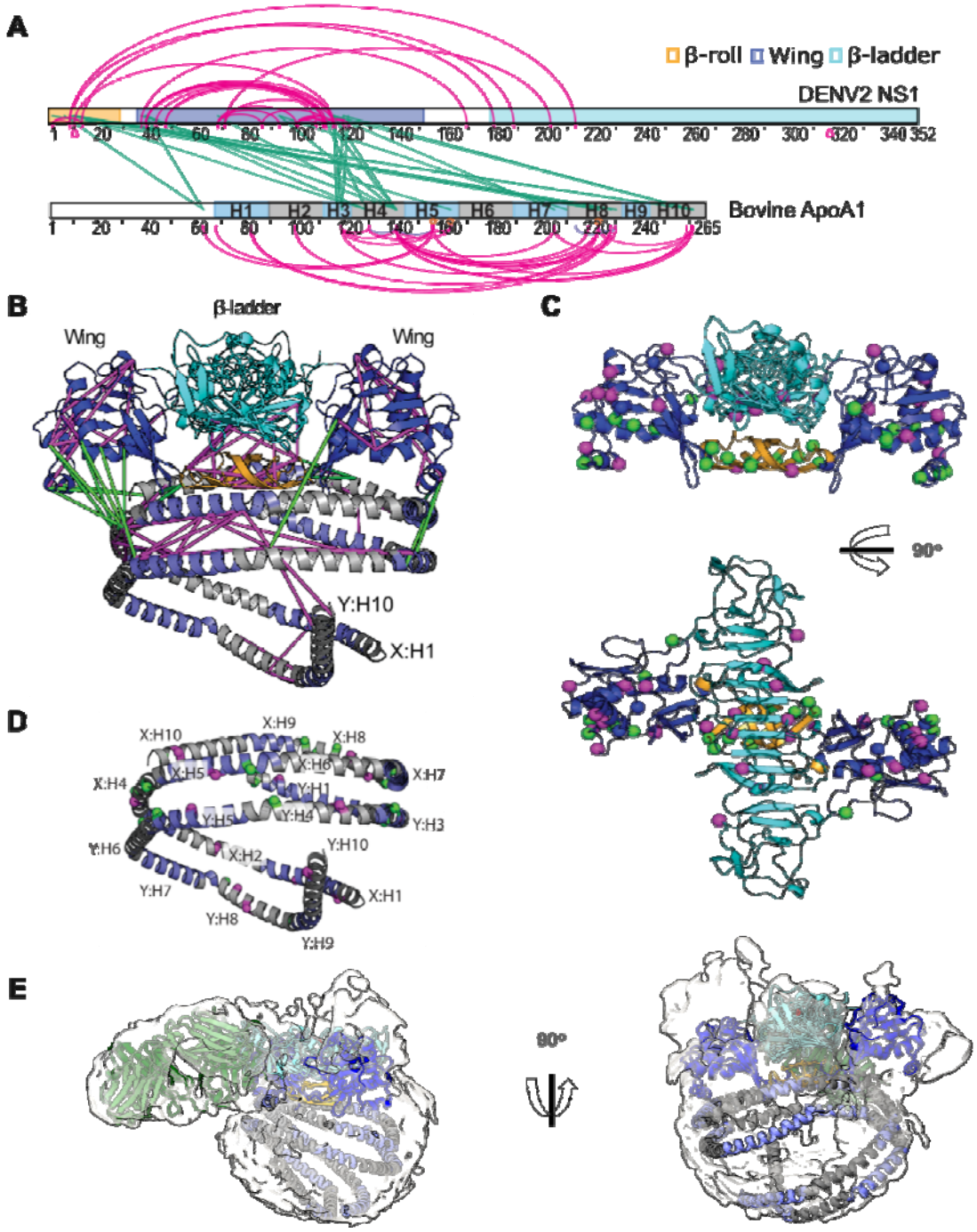

Fig. 4. Interaction sites of sNS1-ApoA1 complex identification by crosslinking mass spectrometry. (A) The intramolecular linkages in sNS1 or ApoA1 (magenta) and intermolecular linkages between sNS1 and ApoA1 (green) identified are as shown and in **(B)** the overall model interpretation within the cross-linker theoretical distance cut-off at =< 30 Å as depicted. **(C)** Intramolecular (magenta) and intermolecular (green) crosslinking sites depicted as spheres on sNS1wt cartoon model and coloured by its three domains, namely the beta-roll (orange), wing (blue), and β-ladder (cyan), and **(D)** ApoA1 dimer cartoon model with its conserved helices as labelled coloured in intervals of grey and light purple. **(E)** Rigid-body fitting of the overall model into the Fab56.2:sNS1wt:HDL density map in grey and contoured at 0.17.